# CHAPTER 2

# ENHANCING THE THERMOELECTRIC PERFORMANCE OF SELF-DEFECT TiNiSn: A FIRST-PRINCIPLES CALCULATION

## Introduction

Defect engineering with self-doping and guest-doping are crucial techniques for improving the performance of thermoelectric (TE) materials (Fu et al., 2015, p. 8144; Li, Xiao, Zhu & Xie, 2016, pp. 14810–14819; Savory, Ganose & Scanlon, 2017, pp. 5156–5167; Yonggang, Zhang & Zunger, 2017, p. 085201). The Seebeck coefficient ($S$), electrical conductivity ($\sigma$), and thermal conductivity ($\kappa$) are the main indicators of TE performance, which are combined to calculate a dimensionless figure of merit ($ZT$), $ZT = S^2\sigma T/\kappa$, where $T$ is absolute temperature (Aswal, Basu & Singh, 2016, pp. 50–67). A high $ZT$ value requires a suitable carrier concentration ($c_{n,p}$) (Snyder & Toberer, 2011, pp. 101–110). The $c_{n,p}$ could be tuned by defect engineering, as $c_{n,p} \propto N_{\mathrm{site}}\exp\left(E_f/(k_{\mathrm{B}}T)\right)$, where $c_{n,p}$ is the carrier concentration, $E_f$ is the defect formation energy, and $N_{\mathrm{site}}$ is the number of defect sites (Eibl, Nielsch, Peranio & Völklein, 2015). The half-Heusler alloy, TiNiSn, is a strong candidate TE material due to its low cost, non-toxic nature, and high $ZT$ in the intermediate to high temperature range. The high $ZT$ value of 0.4 of TiNiSn (Muta, Kanemitsu, Kurosaki & Yamanaka, 2009, pp. 50–55) can be increased above 1.0 by guest-doping (Sakurada & Shutoh, 2005, p. 082105; Rogl et al., 2017, pp. 336–348). The self-defect states of TiNiSn have been studied by first-principles

calculations. Hazama et al. (2010, pp. 1549–1553; 2011, p. 063710) have reported that Ni–defects could reduce the value of $\kappa$ and enhance the power factor (*PF*, $S^2\sigma$). Kirievsky et al. (2013, pp. 247–254) have explained excess Ni in the unit cell could result in a Ni–rich half–Heusler phase, which generates disorder in the $TiNi_{2-X}Sn$ phase due to the Ni vacancies. In addition, the Ni excess included Ni atoms in interstitial tetrahedral sites not available to the $TiNi_2Sn$ full–Heusler alloy (Douglas, Chater, Brown, Pollock & Seshadri, 2014, p. 163514). Wambach et al. (2016, p. 1500208) have studied the defect formation energy of self–defects in TiNiSn. They investigated the TE properties of the Ti–Ni–Sn system with different phases, such as TiNiSn, $Ti_2Sn_3$, $Ti_6Sn_5$, $Ti_5NiSn_3$, $Ti_2Ni$, TiNi, $TiNi_3$, $Ti_2Ni_2Sn$, $Ni_3Sn$, $TiNi_2Sn$, $Ni_3Sn_2$, and $Ni_3Sn_4$. They found that the TE performance was improved by increasing the amount of Sn in the Ti–Ni–Sn system. However, the electronic structure and TE properties of self–defect TiNiSn have not been reported. In this study, we propose to enhance the TE performance of TiNiSn by self–defects. The self–defects, such as self–vacancies (Ti–vac, Ni–vac, Sn–vac), self–substitutions ($Ti_{Ni}$, $Ti_{Sn}$, $Ni_{Ti}$, $Ni_{Sn}$, $Sn_{Ti}$, $Sn_{Ni}$), and self–interstitials (Ti–int, Ni–int, Sn–int) were designed and identified by the stability of point defect configurations via the defect formation energy. The electronic structure and TE properties were calculated using density functional theory and the Boltzmann transport theory framework.

## Computational details

The stability of point defect configurations can be investigated by evaluating the defect formation energy, $E_f(D^q)$, as in the equation: (Van de Walle & Neugebauer, 2004, pp. 3851–3879; González–Romero & Meléndez, 2018, pp. 536–546)

$$E_f(D^q) = E^q_{\mathrm{defect}} - E_{\mathrm{perfect}} - \sum_{\mathrm{X}} n_{\mathrm{X}}(E_{\mathrm{X}} + \mu_{\mathrm{X}}) + qE_{\mathrm{F}}, \quad (50)$$

where $E^q_{\mathrm{defect}}$ is the total energy of the defect structure with the charge defect $q$. $E_{\mathrm{perfect}}$ is the total energy of the perfect structure. $E_{\mathrm{X}}$, $\mu_{\mathrm{X}}$, and $n_{\mathrm{X}}$ are the total energy of the pure element, chemical potential, and the number of atoms of $\mathrm{X}$, respectively. $E_{\mathrm{F}}$ is the Fermi energy. For $n_\alpha$, the positive value (+) is added while negative value (–) is removed from an atom, respectively. $E^q_{\mathrm{defect}}$ and $E_{\mathrm{perfect}}$ are necessarily obtained from the supercell calculation (Freysoldt et al., 2014, p. 253). We use the TiNiSn conventional cell with 2×2×2 unit cells and 96 atoms (Ti = 32, Ni = 32, Sn = 32) for the supercell calculation. The neutral $E_f$ of TiNiSn can be calculated with the following equations:

$$E_f(\mathrm{V_X}) = E(\mathrm{V_X}) - E(\mathrm{TiNiSn}) + E(\mathrm{X}) + \mu_{\mathrm{X}}, \quad (51)$$

$$E_f(\mathrm{X_{Ti}}) = E(\mathrm{X_{Ti}}) - E(\mathrm{TiNiSn}) - E(\mathrm{X}) + E(\mathrm{Ti}) - \mu_{\mathrm{X}} + \mu_{\mathrm{Ti}}, \quad (52)$$

$$E_f(\mathrm{X_{Ni}}) = E(\mathrm{X_{Ni}}) - E(\mathrm{TiNiSn}) - E(\mathrm{X}) + E(\mathrm{Ni}) - \mu_{\mathrm{X}} + \mu_{\mathrm{Ni}}, \quad (53)$$

$$E_f(\mathrm{X_{Sn}}) = E(\mathrm{X_{Sn}}) - E(\mathrm{TiNiSn}) - E(\mathrm{X}) + E(\mathrm{Sn}) - \mu_{\mathrm{X}} + \mu_{\mathrm{Sn}}, \quad (54)$$

$$E_f(\mathrm{int_X}) = E(\mathrm{int_X}) - E(\mathrm{TiNiSn}) - E(\mathrm{X}) - \mu_{\mathrm{X}}, \quad (55)$$

where $E_f(\mathrm{V_X})$ is the defect formation energy of an atom X vacancy. $E_f(\mathrm{X_{Ti}})$, $E_f(\mathrm{X_{Ni}})$, and $E_f(\mathrm{X_{Sn}})$ are the defect formation energies of an X atom substitution in a Ti–, Ni–, and Sn–site, respectively. $E_f(\mathrm{int_X})$ is the defect formation energy of an X atom interstitial in TiNiSn. $E(\mathrm{Ti}), E(\mathrm{Ni})$, and $E(\mathrm{Sn})$ are the total energies of elements Ti, Ni, and Sn.

The chemical potential, $\mu_{\mathrm{X}}$ (X = Ti, Ni, Sn), can be determined from chemical potential limits analysis (McNaught & McNaught, 1997); Buckeridge, Scanlon, Walsh & Catlow, 2014, pp. 330–338). The enthalpy of formation of TiNiSn can be expressed as:

$$\mu_{\mathrm{Ti}} + \mu_{\mathrm{Ni}} + \mu_{\mathrm{Sn}} = \mu_{\mathrm{TiNiSn}} = \Delta H_f(\mathrm{TiNiSn}), \quad (56)$$

where $\mu_{\mathrm{TiNiSn}}, \mu_{\mathrm{Ti}}, \mu_{\mathrm{Ni}}$, and $\mu_{\mathrm{Sn}}$ are the chemical potential of TiNiSn, Ti, Ni, and Sn, respectively. $\Delta H_f(\mathrm{TiNiSn})$ is the enthalpy of formation of TiNiSn which can be expressed as:

$$\Delta H_f(\mathrm{TiNiSn}) = E(\mathrm{TiNiSn}) - [E(\mathrm{Ti}) + E(\mathrm{Ni}) + E(\mathrm{Sn})]. \quad (57)$$

For a compound $A_nB_nC_n$, the enthalpy of formation can be described by the equation:

$$\Delta H_f(A_nB_nC_n) = E_{A_nB_nC_n}(\mathrm{bulk}) - \sum_{\alpha}^{A,B,C} n_{\alpha} E_{\alpha}(\mathrm{bulk}). \quad (58)$$

The $\Delta H_f$ of the Ti–Ni–Sn system was calculated by using the crystal structure as determined from experimental data (Douglas et al., 2014, p. 043720; Romaka, et al., 2013, pp. 103–112) and the Materials Project (Jain et al., 2013, p. 011002). The crystal structure data of the Ti–Ni–Sn system is composed of the TiNiSn (SG 216), $TiNi_3$ (SG 194), $Ti_2Sn$ (SG 194), $Ti_2Sn_3$ (SG 64), $Ti_3Sn$ (SG 194), $Ti_6Sn_5$ (SG 194), TiNi (SG 11), $Ti_5Sn_3$ (SG 193), NiSn (SG 55), $Ni_3Sn_2$ (SG 62), and $Ni_3Sn_4$ (SG 12) phases, where SG is a space group number. The chemical potential of Ti, Ni, and Sn were analyzed by the chemical potential limits analysis program (CPLAP) (Buckeridge et al., 2014, pp. 330–338) according to Equation (7), as shown in Figure 11.

In order to know the defect stability of a point defect configuration, the possible configurations of $E_f$ were calculated. For example, a Ti vacancy with thirty–two possibilities can be expressed as:

$$\begin{aligned} E_f(\mathrm{V}_{\mathrm{Ti(site\ 1)}}) &= E(\mathrm{V}_{\mathrm{Ti(site\ 1)}}) - E(\mathrm{TiNiSn}) + E(\mathrm{Ti}) + \mu_{\mathrm{Ti}} \\ E_f(\mathrm{V}_{\mathrm{Ti(site\ 2)}}) &= E(\mathrm{V}_{\mathrm{Ti(site\ 2)}}) - E(\mathrm{TiNiSn}) + E(\mathrm{Ti}) + \mu_{\mathrm{Ti}} \\ &\vdots \\ E_f(\mathrm{V}_{\mathrm{Ti(site\ 32)}}) &= E(\mathrm{V}_{\mathrm{Ti(site\ 32)}}) - E(\mathrm{TiNiSn}) + E(\mathrm{Ti}) + \mu_{\mathrm{Ti}} \end{aligned}, \quad (59)$$

where, Ti(site 1), Ti(site 2),..., and Ti(site 32) represent the possible atomic configuration positions of the Ti vacancy in the TiNiSn $2\times2\times2$ unit cells. After that, we considered the point defect configuration with the lowest $E_f$ value.

The TE properties are based on *S*, the electrical conductivity as a function of relaxation time ($\sigma/\tau$), and *PF* which can be calculated using Boltzmann transport theory with the constant scattering time approximation (CSTA) and Fourier interpolation of the calculated bands, based on the BoltzTraP code (Madsen & Singh, 2006, pp. 67–71). The *S* and $\sigma$ tensors were calculated as:

$$S_{\alpha\beta}(T,\mu) = \frac{1}{eT\sigma_{\alpha\beta}(T,\mu)} \int \bar{\sigma}_{\alpha\beta}(\varepsilon)(\varepsilon-\mu)\left[-\frac{\partial f_0(T,\varepsilon,\mu)}{\partial\varepsilon}\right] d\varepsilon, \quad (60)$$

$$\sigma_{\alpha\beta}(T,\mu) = \frac{1}{\Omega} \int \sigma_{\alpha\beta}(\varepsilon)\left[-\frac{\partial f_0(T,\varepsilon,\mu)}{\partial\varepsilon}\right] d\varepsilon, \quad (61)$$

where $e$ is the charge of an electron, $\varepsilon$ is an eigen–energy of each band structure, $f_0$ is the Fermi–Dirac distribution function, and $\Omega$ is reciprocal space volume.

The total energies were calculated by the plane wave self–consistent field (PWSCF). The PWSCF is based on a density functional theory (DFT) framework (Hohenberg & Kohn, 1964, p. B864; Kohn & Sham, 1965, p. A1133) and is implemented in the Quantum ESPRESSO package (Giannozzi et al., 2009, p. 395502; Giannozzi et al., 2017, p. 465901). The optimized values were obtained by using a 2×2×2 Monkhorst–Pack *k*–mesh Brillouin zone (BZ) integration, lattice constant *a* = 0.5951(3) nm, kinetic energy cutoff of 340 eV, and convergence threshold of $1\times10^{-8}$ for the supercell calculations. The CIF2Cell package (Björkman, 2011, pp. 1183–1186) was employed determine the optimal Monkhorst–Pack *k*–mesh BZ for the Ti–Ni–Sn system. The exchange–correlation energy function was used under the ultrasoft–pseudopotential based on the Perdew–Burke–Ernzerhof (PBE) functional (Perdew, 1996, p. 3865) and generalized gradient approximation (GGA) (Rappe, Rabe, Kaxiras & Joannopoulos, 1990, p. 1227). The Broyden–Fletcher–Goldfarb–Shanno (BFGS) quasi–Newton algorithm and a force convergence threshold of $1\times10^{-3}$ were employed in the relaxed structure calculation.

## Results and Discussion

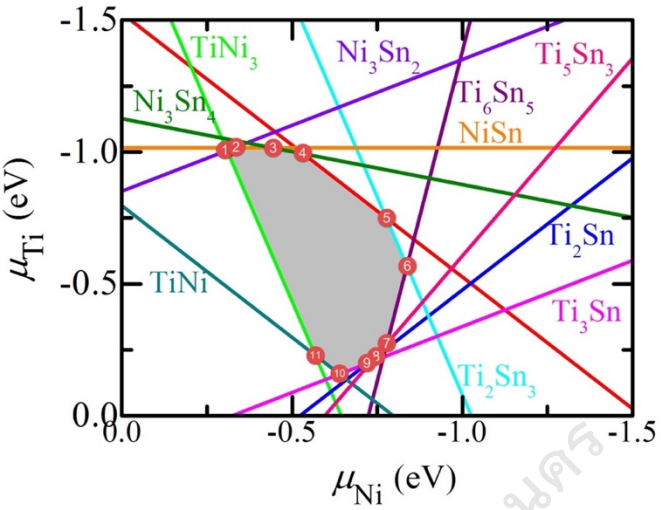


Figure 11 The chemical potential region of stability for Ti–Ni–Sn in 2D space which spanned by $\mu_{Ni}$ and $\mu_{Ti}$. The eleven points are discussed in the results and discussion section.

Table 2 Chemical potential of Ti, Ni, and Sn with the completing phases referred to in Figure 11

| point | $\mu_{Ti}$ (eV) | $\mu_{Ni}$ (eV) | $\mu_{Sn}$ (eV) | Completing phases |
|---|---|---|---|---|
| 1 | –1.0056 | –0.3092 | –0.2117 | $TiNi_3$ + $Ni_3Sn_2$ |
| 2 | –1.0161 | –0.3302 | –0.1802 | NiSn + $Ni_3Sn_2$ |
| 3 | –1.0161 | –0.4431 | –0.0673 | NiSn + $Ni_3Sn_4$ |
| 4 | –0.9937 | –0.5328 | 0 | $Ni_3Sn_4$ + TiNiSn |
| 5 | –0.7502 | –0.7763 | 0 | $Ti_2Sn_3$ + TiNiSn |
| 6 | –0.5674 | –0.8372 | –0.1219 | $Ti_2Sn_3$ + $Ti_6Sn_5$ |
| 7 | –0.2727 | –0.7783 | –0.4756 | $Ti_6Sn_5$ + $Ti_5Sn_3$ |
| 8 | –0.2202 | –0.7433 | –0.5630 | $Ti_2Sn$ + $Ti_5Sn_3$ |
| 9 | –0.1992 | –0.7223 | –0.6050 | $Ti_2Sn$ + $Ti_3Sn$ |
| 10 | –0.1575 | –0.6389 | –0.7301 | $Ti_3Sn$ + TiNi |
| 11 | –0.2280 | –0.5685 | –0.7301 | $TiNi_3$ + TiNi |

The chemical potential region is shown in Figure 11 as a function of $\mu_{\mathrm{Ti}}$ and $\mu_{\mathrm{Ni}}$ for the Ti–Ni–Sn system. The highlighted area (gray) is the thermodynamically stable region (Buckeridge et al., 2014, pp. 330–338; Wang et al., 2014, pp. 3411–3417), thus TiNiSn can be grown in this area (Romaka et al., 2013, pp. 103–112) while the rest of the region is unstable. The Ni–rich (Ti–rich, Sn–poor) phases appear at points 1 and 2. The Sn–rich phase can be observed at points 3 to 6. Points 7 to 11 indicate Ti–rich (Ni–rich and Sn–poor) phases. In addition, the chemical potential line of the TiNi phase is different than that reported in previous works. Wanbach *et al.* (2016, p. 1500208) added the $Ti_2Ni_2Sn$ phase, while Yonggang *et al.* (2017, p. 085201) included the $TiNi_2Sn$ phase to complete the stable chemical potential region of growth conditions. On the other hand, the TiNi result is similar to the $Ti_2Ni_2Sn$ phase due to the reaction $\mathrm{Ti_2Ni_2Sn} \leftrightarrow \mathrm{TiNi} + \mathrm{TiNiSn}$. Our calculation of eleven different points for the different growth environments and their corresponding phases are illustrated in Table 2.

In order to see the stability of $E_f$ under different growth conditions, we used the chemical potential from Table I combined with equations (2) – (6). The calculated $E_f$ values of self–defect TiNiSn in different growth environments are illustrated in Figure 12. The Ni–vac, $Sn_{Ti}$, $Sn_{Ni}$, Ni–int, and Ti–int exhibited mostly stable self–defects due to their low $E_f$ values. Our calculated energies for Ni–vac and Ni–int have been confirmed by experimental data (Hazama et al., 2011, p. 063710; Douglas et al., 2014, p. 163514). Not all self–defect energies can be confirmed due to a lack of experimental data. However, our calculated $E_f$ values are in good agreement with previous work (Wanbach et al., 2016, p. 1500208). Under different growth conditions, we found that the Ni–vac, Ni–int, and Ti–int defects are stable, but the $Ti_{Ni}$ defect exhibits stability in the Sn–rich region. In case of Sn–defects, the $Sn_{Ti}$ defect showed the lowest $E_f$ in the Ni–rich region, while the $Sn_{Ni}$ defect exhibited the lowest

$E_f$ under Ti-rich conditions. Therefore, the Sn-int defect became stable in the Ti-rich phase.

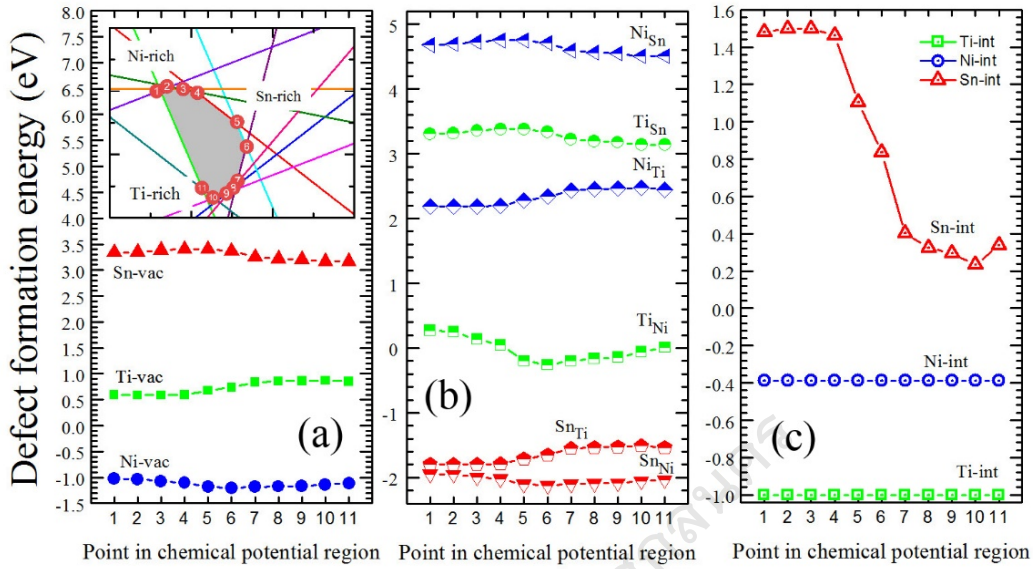


Figure 12 The calculated defect formation energy of self-defect TiNiSn including self-vacancies (a), self-substitutions (b), and self-interstitials (c) at Fermi energy = 0. The inset shows the chemical potential and completing phases which are described in Table 2.

The calculated $E_f$ values suggest that the Sn-vac, Ti-vac, $Ni_{Sn}$, $Ti_{Sn}$, $Ni_{Ti}$, and Sn-int defects are not favorable. We focused on the electronic and TE properties of the favorable self-defects, such as Ni-vac, $Ti_{Ni}$, $Sn_{Ti}$, $Sn_{Ni}$, Ti-int, and Ni-int. The calculated total density of states (TDOS) is illustrated in Figure 13. The energies are composed of the negative value of the valence band, positive value of the conduction band, and $E_F$, respectively. The TDOS of TiNiSn shows an energy gap of 0.46 eV, which is in good agreement with values reported in the literature (Douglas et al., 2014, p. 043720; Wang et al., 2009, p. 013709). The energy gap was decreased from 0.46 to 0.21 eV by the Ni-vac. At the $E_F$ state, the TDOS is increased by the $Ti_{Ni}$,

$Sn_{Ti}$, $Sn_{Ni}$, Ti–int, and Ni–int defects, as shown in Figure 13(b). This implies that the self–defects have provided an electron pocket due to the self–substitution and self–interstitial defects. The value of $S$ depends on the TDOS($E_F$) and $\sigma$, and can be expressed as:

$$S \propto \frac{1}{\mathrm{DOS}(\mathrm{E_F})} \frac{\partial[\mathrm{DOS}(\mathrm{E_F})]}{\partial \mathrm{E_F}}, \tag{13}$$

$$S = \frac{\pi^2 k_B^2 T}{3e} \frac{\partial[\ln \sigma(\mathrm{E_F})]}{\partial \mathrm{E_F}}, \tag{14}$$

where $k_B$ is Boltzmann's constant.

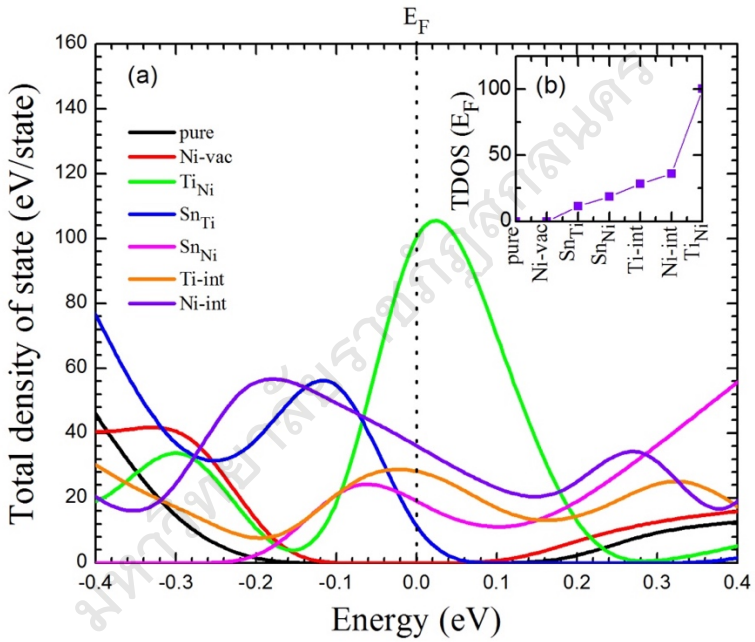


Figure 13 Total density of state versus energy (a) and the total density of state at Fermi energy (b) for TiNiSn, Ni–vac, $Ti_{Ni}$, $Sn_{Ti}$, $Sn_{Ni}$, Ti–int, and Ni–int.

As we know, DFT calculations are performed at ground state with zero temperature. In order to investigate TE properties, we employed the BoltzTraP code (Madsen & Singh, 2006, pp. 67–71) with a 6×6×6 Monkhorst–Pack *k*–mesh BZ integration to calculate the transport properties from 300 to 1000 K. The relationship between the TDOS($E_F$) and the temperature is illustrated in Figure 14. We observed

that the TDOS($E_F$) of TiNiSn, Ni–vac, and $Sn_{Ti}$ has a small value from 300 to 700 K and becomes large at temperatures above 700 K due to the increased size of the electron pocket. The TDOS($E_F$) of $Ti_{Ni}$ showed a small value at 300 K and strongly increased with increasing temperature. The $Sn_{Ni}$, Ti–int, and Ni–int defects exhibited a large value of TDOS($E_F$) at 300 K and remained constant at high temperatures.

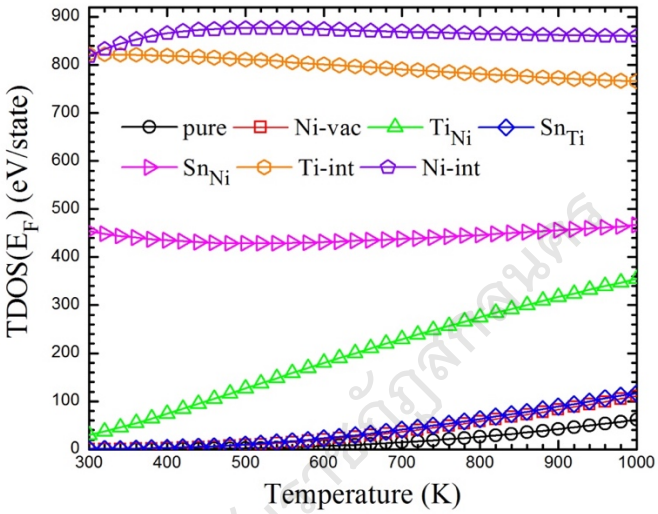


Figure 14 Total density of states at the Fermi energy versus temperature for TiNiSn, Ni–vac, $Ti_{Ni}$, $Sn_{Ti}$, $Sn_{Ni}$, Ti–int, and Ni–int.

The transport properties are shown in Figure 15 as a function of temperature. Figure 15(a) shows $S$ with a negative value, which suggests an *n*–type TE material (Muta et al., 2009, pp. 50–55). The $S$ of TiNiSn was found to be –317 $\mu V\ K^{-1}$ at 300 K and decreased to –135 $\mu V\ K^{-1}$ at 1000 K, which is consistent with the previous work (Jain et al., 2013, p. 011002). In addition, the value of $S$ is decreased by self–defects with the increase of the TDOS($E_F$). It is clear that the Ti–int and Ni–int defects exhibit metallic behavior because they have a small $S$. The $S$ values of Ni–vac, $Ti_{Ni}$, $Sn_{Ti}$, and $Sn_{Ni}$ are close to that of TiNiSn at 1000 K. The calculated $\sigma/\tau$ values showed behavior similar to $S$. It is observed that the $\sigma/\tau$

values of Ni–vac and $Sn_{Ti}$ are close to that of TiNiSn from 300 – 1000 K. The $\sigma/\tau$ of $Ti_{Ni}$ is more than that of TiNiSn.

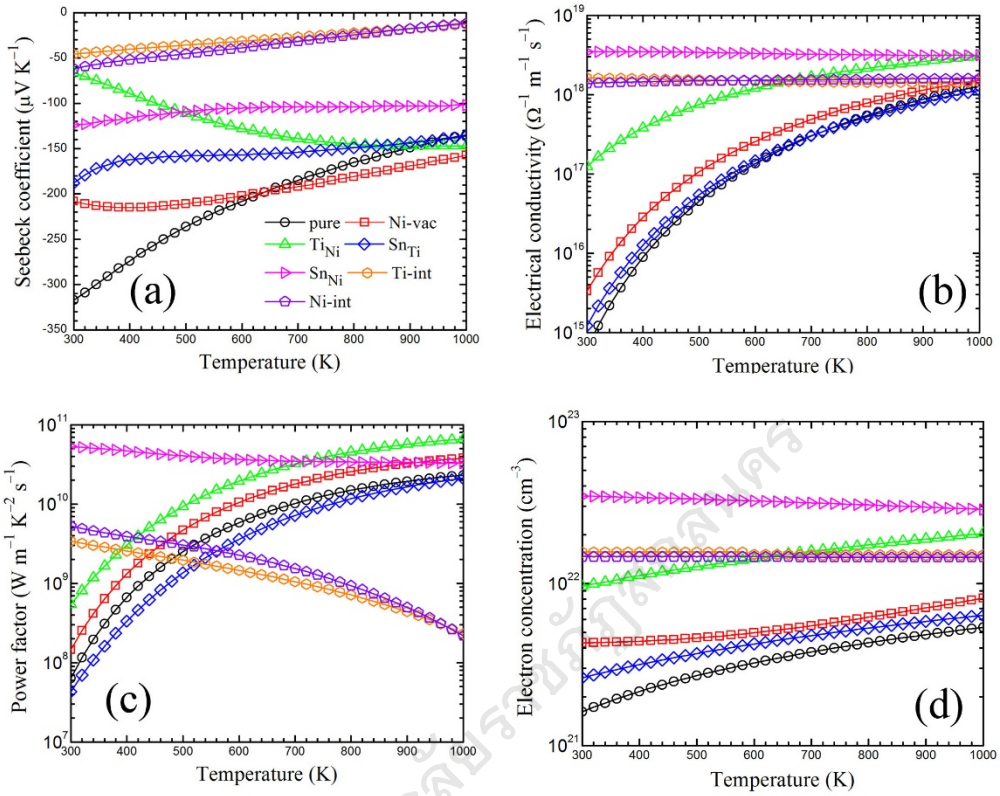


Figure 15 The Seebeck coefficient (a), electrical conductivity (b), power factor, (c), and electron concentration (d) versus temperature for TiNiSn, Ni–vac, $Ti_{Ni}$, $Sn_{Ti}$, $Sn_{Ni}$, Ti–int, and Ni–int.

The $\sigma/\tau$ of $Sn_{Ni}$, Ti–int, and Ni–int exhibited high values at 300 K and remained constant with increasing temperature. In order to determine the calculated $\sigma$ without the scattering $\tau$, experimental electrical conductivity ($\sigma_{exp}$) data is required (Ong, Singh & Wu, 2011, p. 115110), which is rare for self–defects. Alternatively, molecular dynamics simulations with the Green–Kubo relation (MD–GK) could provide an estimate of $\tau$. We have successfully applied this technique to oxide (Rittiruam et al., 2016, pp. 8822–8826) and silicide (Rittiruam, Vora–Ud, Impho & Seetawan, 2015, pp. 61–72) thermoelectric materials. However, many parameters are required

to investigate $\tau$ using MD–GK, such as internal energy, mean square displacement, thermal expansion, heat–flux auto–correlation, and lattice thermal conductivity ($\kappa_{lat}$). Therefore, the theoretical thermal properties of self–defect TiNiSn must be known. We also present the transport properties with the scattering $\tau$.

Table 3 The maximum power factor ($PF_{max}$) for TiNiSn, Ni–vac, $Ti_{Ni}$, $Sn_{Ti}$, $Sn_{Ni}$, Ti–int, and Ni–int.

| | $PF_{max}$ ($W\ m^{-1}\ K^{-2}\ s^{-1}$) | Temperature (K) | Electron concentration ($cm^{-3}$) | Enhanced PF (%) |
|---|---|---|---|---|
| TiNiSn | $2.31\times10^{10}$ | 1000 | $5.36\times10^{21}$ | – |
| Ni–vac | $3.79\times10^{10}$ | 1000 | $8.11\times10^{21}$ | +64.06 |
| $Ti_{Ni}$ | $6.60\times10^{10}$ | 1000 | $2.04\times10^{22}$ | +185.71 |
| $Sn_{Ti}$ | $2.11\times10^{10}$ | 1000 | $6.36\times10^{21}$ | –8.65 |
| $Sn_{Ni}$ | $3.66\times10^{10}$ | 300 | $3.20\times10^{22}$ | +58.44 |
| Ti–int | $1.46\times10^{9}$ | 300 | $1.51\times10^{22}$ | –80.08 |
| Ni–int | $2.27\times10^{9}$ | 300 | $1.46\times10^{22}$ | –90.17 |

The calculated *PF* is illustrated in Figure 15(c). It is clear from Figure 15(c) that the $Sn_{Ni}$ defect has the highest value of *PF* at 300–700 K, while the *PF* of $Ti_{Ni}$ has the highest value at temperatures above 700 K. We observed that the Ni–vac, $Ti_{Ni}$, and $Sn_{Ni}$ defects can enhance the *PF* of TiNiSn at 1000 K. As we know, the TE properties depend on temperature and also on carrier concentration (Aswal et al., 2016, pp. 50–67) [5]. Our calculated electron concentration at 300 K is $1.6 \times 10^{21}$ $cm^{-3}$ for TiNiSn, $4.3 \times 10^{21}$ $cm^{-3}$ for Ni–vac, $9.62 \times 10^{21}$ $cm^{-3}$ for $Ti_{Ni}$, $2.62 \times 10^{21}$ $cm^{-3}$ for $Sn_{Ti}$, $3.46 \times 10^{22}$ $cm^{-3}$ for $Sn_{Ni}$, $1.56 \times 10^{22}$ $cm^{-3}$ for Ti–int, and $1.46 \times 10^{22}$ $cm^{-3}$ for Ni–int. It was observed that the electron concentration increased with Ni–vac, $Ti_{Ni}$, $Sn_{Ti}$, $Sn_{Ni}$, Ti–int, and Ni–int. The contribution from the electron transport means that *PF* can be

enhanced by tuning the electronic structure, specifically the DOS at $E_F$ (DOS($E_F$)) and the electron concentration. The maximum *PF* with percentage increase is shown in Table 3.

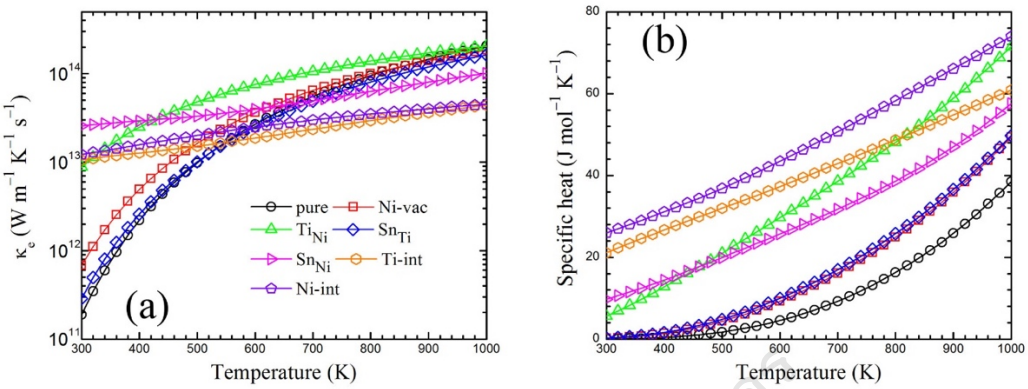


Figure 16 The electron thermal conductivity (a) and specific heat (b) versus temperature for TiNiSn, Ni–vac, $Ti_{Ni}$, $Sn_{Ti}$, $Sn_{Ni}$, Ti–int, and Ni–int.

In order to investigate the $ZT$, $\boldsymbol{\kappa}$ is a very important parameter. However, the procedure for calculating $\boldsymbol{\kappa}$ requires high–performance computing, as discussed above. The results of our thermal calculations were obtained by BoltzTraP (Madsen & Singh, 2006, pp. 67–71) which considers the electron thermal conductivity ($\boldsymbol{\kappa_e/\tau}$) and specific heat, as shown in Figure 16. As we know, the total thermal conductivity is composed of $\boldsymbol{\kappa_{lat}}$ and $\boldsymbol{\kappa_e}$. For TiNiSn, the contribution from $\boldsymbol{\kappa_{lat}}$ is greater than that of $\boldsymbol{\kappa_e}$ at low temperatures. Then, the $\boldsymbol{\kappa_e}$ becomes the main contributor at intermediate temperatures. The $Sn_{Ni}$, Ti–int, and Ni–int defects showed $\boldsymbol{\kappa_e/\tau}$ values less than that of TiNiSn at 600 – 1000 K. The Ni–vac and $Sn_{Ti}$ defects are suitable for controlling the value of $\boldsymbol{\kappa_e/\tau}$. Experimental data for the $\boldsymbol{\kappa}$ of self–defects is quite rare. Thus far, Hazama et al. have reported that Ni–defects could reduced the thermal conductivity at 0 – 300 K (Hazama et al., 2011, p. 063710). As reported in a previous work (Rittiruam et al., 2016, pp. 8822–8826), the specific heat of $SrTiO_3$ was increased by doping with rare earth elements. The rare earth could reduce the $\boldsymbol{\kappa_{lat}}$ of $SrTiO_3$. The

specific heat was increased by self–defects, which implies that the $\kappa_{\mathbf{lat}}$ of TiNiSn can be decreased by self–defects, as shown in Figure 16(b).

## Summary

The self–defects of TiNiSn, including vacancies, substitutions, and interstitials, were identified by the defect formation energy. It was found that the Ni–vac, $Ti_{Ni}$, $Sn_{Ti}$, $Sn_{Ni}$, Ti–int, and Ni–int defects are most favorable for the stability of point defect configurations. The self–defects induced a pocket of high electron density in the DOS at $E_F$ and increased the electron concentration from ~$10^{21}$ $cm^{-3}$ – ~$10^{22}$ $cm^{-3}$. The *PF* values of Ni–vac, $Ti_{Ni}$, and $Sn_{Ni}$ showed a great enhancement, which was improved by the $\sigma/\tau$ value. In addition, the self–defects lead to increased specific heat, which is implied that the $\kappa_{\mathbf{lat}}$ of TiNiSn tend to boost. Our study yields that the Ni–vac and $Sn_{Ni}$ are strong candidates for enhancing the TE performance of TiNiSn half Heusler alloy. However, the $\kappa_{\mathbf{lat}}$ and thermal properties should be determined to investigate the optimized $ZT$ of the self–defect TiNiSn.